

One simulation to have them all: performance of the Bias Assignment Method against N -body simulations

A. Balaguera-Antolínez^{★1,2}, Francisco-Shu Kitaura^{†1,2}, Marcos Pellejero-Ibáñez³, Martha Lippich⁴, Cheng Zhao⁵, Ariel G. Sánchez⁴, Claudio Dalla Vecchia^{1,2}, Raúl E. Angulo^{3,6} and Martín Crocce⁷

¹*Instituto de Astrofísica de Canarias, s/n, E-38205, La Laguna, Tenerife, Spain*

²*Departamento de Astrofísica, Universidad de La Laguna, E-38206, La Laguna, Tenerife, Spain*

³*Donostia International Physics Centre (DIPC), Paseo Manuel de Lardizabal 4, 20018 Donostia-San Sebastian, Spain*

⁴*Max-Planck-Institut für extraterrestrische Physik, Postfach 1312, Giessenbachstr., 85741 Garching, Germany*

⁵*National Astronomy Observatories, Chinese Academy of Science, Beijing, 100012, P.R. China*

⁶*IKERBASQUE, Basque Foundation for Science, 48013, Bilbao, Spain.*

⁷*Institut de Ciències de l'Espai, IEEC-CSIC, Campus UAB, Carrer de Can Magrans, s/n, 08193 Bellaterra, Barcelona, Spain*

8 May 2022

ABSTRACT

In this paper we demonstrate that the information encoded in *one* single (sufficiently large) N -body simulation can be used to reproduce arbitrary numbers of halo catalogues with different phases. To this end we use as a reference one realisation (from an ensemble of 300) of the Minerva N -body simulations and the recently published Bias Assignment Method (BAM, Balaguera-Antolínez et al. 2019) to extract the local and non-local bias linking the halo to the dark matter distribution. We use an approximate (and fast) gravity solver to generate 300 dark matter density fields from the down-sampled initial conditions of the reference simulation and sample each of these fields using the halo-bias and a kernel, both calibrated from the arbitrarily chosen realisation of the reference simulation. We show that the power spectrum, its variance and the three-point statistics are reproduced within $\sim 2\%$ (up to $k \sim 1.0 h\text{Mpc}^{-1}$), $\sim 5\%$ and 10% , respectively. Using a model for the real space power spectrum we show that the covariance matrices obtained from our procedure lead to parameter uncertainties that are compatible within $\sim 1\%$ with respect to those derived from the reference covariance matrix. Our method has the potential to learn from one simulation with moderate volumes and high-mass resolution and extrapolate the information of the bias and the kernel to larger volumes, making it ideal for the construction of mock catalogues for present and forthcoming observational campaigns such as Euclid or DESI.

Key words: cosmology: – theory - large-scale structure of Universe

1 INTRODUCTION

The cosmological volumes explored by current galaxy surveys such as eBOSS (Dawson et al. 2016), DES (The Dark Energy Survey Collaboration 2005), and the unprecedented volumes expected to be probed by forthcoming experiments such as Euclid (Amendola et al. 2016) and DESI (Levi et al. 2013), demand precise and accurate covariance matrices for

galaxy clustering analysis (e.g. Dodelson & Schneider 2013; Taylor et al. 2013; Percival et al. 2014; Paz & Sánchez 2015). The complex evolution underlying a galaxy distribution and galaxy physical processes (e.g. galaxy bias, baryon effects, redshift space distortions) implies the necessity of N -body simulations to construct mock catalogues and generate precise covariance matrices, particularly on small scales. Although this represents the standard approach to assess robust error estimates on cosmological observables, in practice it imposes strong restrictions in terms of computation times and memory requirements. Recently, Lippich et al.

★ balaguera@iac.es

† fkitaura@iac.es

(2019); Colavincenzo et al. (2018) and Blot et al. (2019b) compared different methods to generate mock catalogues and covariance matrices for different statistical probes, showing the limits and potential of different approaches currently available in the literature.

The recently published Bias Assignment Method (BAM) by Balaguera-Antolínez et al. (2019) (Paper I hereafter) has been introduced as an alternative path towards the construction of large number of mock galaxy catalogues. The method exploits the idea of mapping the halo distribution onto an approximated dark matter density field (A-DMDF hereafter), based on measurements of the halo-bias. Although this approach has been explored by previous works such as PThalos (Scoccimarro & Sheth 2002), MoLUSC (Sousbie et al. 2008), PATCHY (Kitaura et al. 2014), QPM (White et al. 2014), EZ-MOCKS (Chuang et al. 2015) and HALOGEN (Avila et al. 2015), the key difference is that BAM does not assume any special analytical form for the halo-bias relation. Instead, the method makes use of the statistical interpretation of the halo-bias (e.g. Dekel & Lahav 1999) and extracts it in the form of a parameter-free probability distribution from the combination of the A-DMDF and a reference catalogue of tracers, here dark matter haloes (DMH hereafter), obtained from *one* high resolution N -body simulation (see e.g. Schneider et al. 2017, for a similar approach to create weak lensing maps). This allows us to include almost all possible non-linearities and stochastic features present in the halo-bias. Another key aspect of BAM is that the A-DMDFs are obtained by evolving the initial conditions (ICs hereafter) of the reference N -body simulation using approximated gravity solvers such as FastPM (Feng et al. 2016) or the Augmented Lagrangian perturbation theory (ALPT, Kitaura & Hess 2013), thus providing a good template for the large-scale distribution of the dark matter density field (DMDF hereafter) while accounting for the bias introduced by the approximate representation of the DMF on small scales. This is achieved by means of a multi-dimensional bias relation beyond the univariate PDF, as suggested by Weinberg (1992) (see also Leclercq et al. (2013)).

The BAM approach has been envisaged to generate mock catalogues with a power spectrum that replicates, to percent precision, that of the high-resolution halo distribution used as a reference. This, together with the description of the method, has been shown and discussed in Paper I. In this article we want to go deeper into the validation of BAM, by assessing its capability to generate independent realisations of mock catalogues based on the calibration of the halo-bias obtained from *only one realisation of the reference simulation*. In particular, we quantify such capability by comparing relevant summary statistics in Fourier space (such as the two-point statistics by means of the halo power spectrum, and the three-point represented by the halo bispectrum) and by testing the performance of the covariance matrix of the power spectrum from these catalogues against that of an ensemble of reference N -body simulations in the framework of a likelihood analysis. We show that our method can generate covariance matrices that yield errors in model parameters, which are compatible within $\sim 1\%$ with respect to those derived from a set of reference N -body simulations, giving BAM the potential to become one of the standard techniques to generate mock catalogues for large-scale structure analysis.

The outline of this paper is as follows. In § 2 we describe the procedure to generate ensembles of halo density fields with BAM. In § 3 we show the comparison of the statistical properties of a set of mocks created with BAM against that from the reference ensemble. In particular, we check the behaviour of the mocks in terms of the two point statistics in Fourier space, as well as at the level of a likelihood analysis based on the power spectrum. We finish with discussion and conclusions.

2 METHODOLOGY

This section presents a deeper exposition of the procedures followed within BAM, already introduced in Paper I. In order to facilitate the understanding of the procedure, we have depicted the main steps in the flow-chart of Fig. 1, whose notation we will follow along this paper.

2.1 Inputs

The main inputs of BAM are, on one side, one realisation of the ICs of a high-resolution N -body simulation and, on the other side, the halo catalogue corresponding to that particular realisation of the reference simulation. As the reference we have adopted the Minerva simulations (Grieb et al. 2016), that consists in a set of $N_{\text{sim}} = 300$ realisations of dark matter and dark matter halo distributions, each embedded in a cubic box of $L_{\text{box}} = 1.5h^{-1}$ Gpc side. Dark matter haloes are identified with a standard Friends-of-Friends (FoF) algorithm at redshift $z = 1$, and subjected to an unbinding procedure (Springel et al. 2001), in which particles with positive total energy are removed and haloes artificially linked by FoF are separated. The minimum halo mass is $\sim 2.7 \times 10^{12} h^{-1} M_{\odot}$.

2.2 Calibration

The calibration process in BAM aims at delivering two products, namely, a kernel, and a halo-bias, with which a set of halo mock catalogues are to be constructed. The role of the kernel is to correct for any effective large scale contributions which may come from non-local bias dependencies not modeled in BAM (see e.g. McDonald & Roy 2009), on the one hand, and to correct for any aliasing effects caused by the representation of the DMF and the halo distribution on a mesh with respect to the original halo finding algorithm used to construct the reference catalogue.

As depicted in Fig. 1, the calibration procedure starts with a down-sampling of the ICs from a high resolution white noise into a low resolution version thereof. For the current set-up we have transformed the ICs from a 1000^3 into a 500^3 resolution. This new white noise is transformed to Fourier space and multiplied by the squared-root of the linear matter power spectrum in spherical shells, $P_{\text{lin}}(|\mathbf{k}|)$, evaluated at the initial redshift of the simulations. The resulting field is evolved up to $z = 1$ to generate the A-DMDF $\delta_{\text{dm}}^i(\mathbf{r})$. This is achieved by using ALPT (Kitaura & Hess 2013) combined with the phase-space mapping technique (Abel et al. 2012; Hahn et al. 2013), the latter being proven to be a key ingredient to obtain a reasonable three-point statistics of the

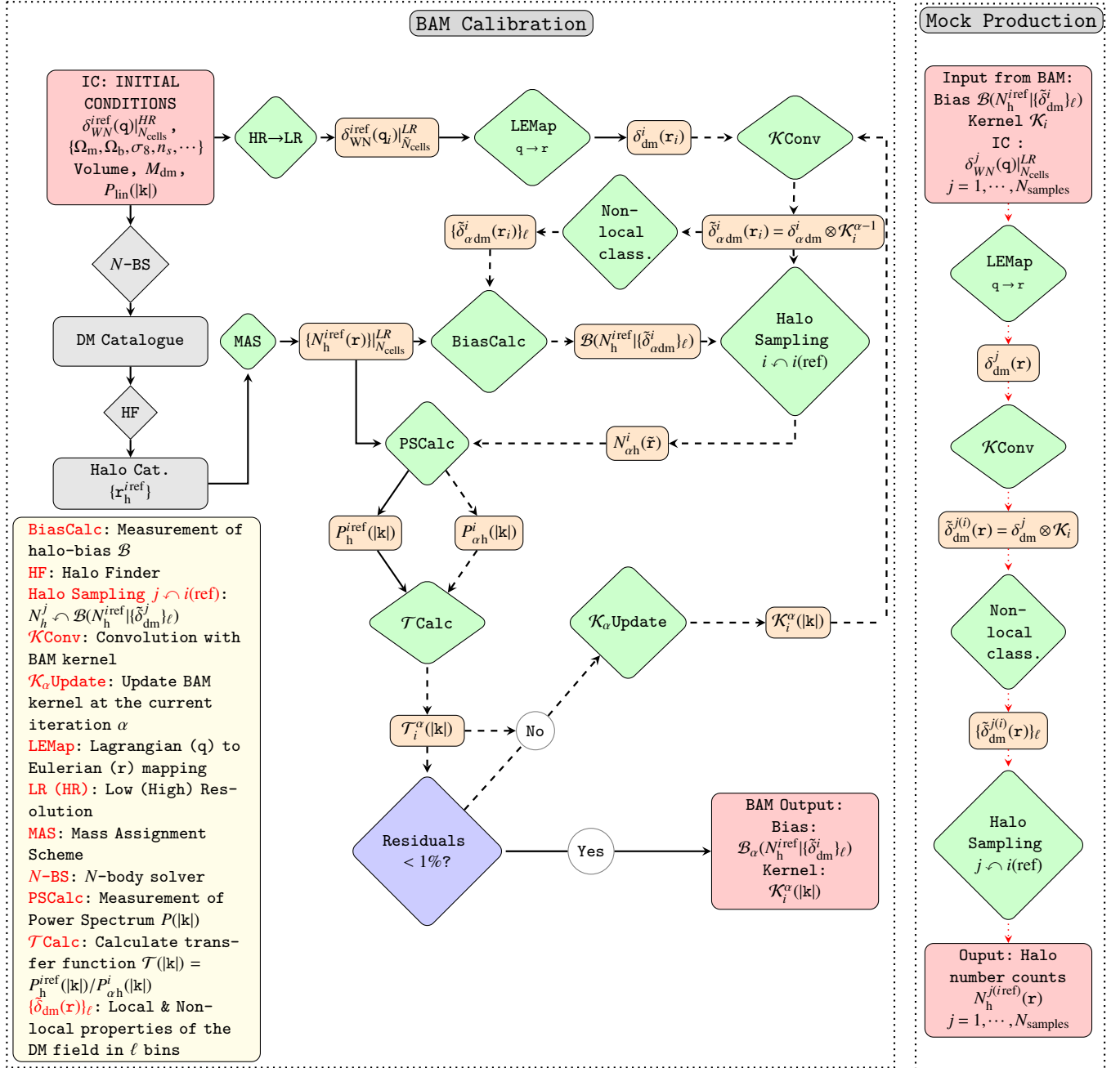


Figure 1. Flow-chart representing the operations performed within BAM. On the left-hand side box (BAM Calibration) we show the iterative process developed in order to calibrate the kernel \mathcal{K} and the halo-bias using *one* realisation of a halo catalogue from the reference simulation, $\{r_{\text{h}}^{i\text{ref}}\}$, in combination with a dark matter density field obtained from the approximated gravity solver with the corresponding initial conditions $\delta_{WN}^{i\text{ref}}(\mathbf{q})$. Solid line arrows denote the process involving the reference N -body simulation, performed once. Dotted-line arrows denote the iterative process, which finishes once the relative residuals (see text) are below 1%. The index α is assigned to quantities being updated within the iterative process, while i identifies a white noise from the reference simulation. For the first iteration the kernel is $\mathcal{K}_i^{\alpha=0}(|\mathbf{k}|) = 1$. The right hand side box (Mock Production) depicts the process followed to generate mock halo density fields based on the outputs of BAM.

mock haloes within BAM, at least for the halo-mass resolution of our reference simulation (Paper I, Pellejero-Ibañez et al., in preparation). The A-DMDF is generated using the cloud-in-cell mass assignment scheme.

The next step consists in the measurement of the halo-bias and the so-called BAM-kernel \mathcal{K} . Starting with the halo-bias, BAM adopts its stochastic interpretation (see e.g. Dekel

& Lahav 1999; Sigad et al. 2000) and measures the probability of finding a number of DMH, N_{h} , within the volume of a LR cell, conditional to the set of local and non-local properties of the A-DMDF in that particular cell. We denote the latter properties as $\{\delta_{\text{dm}}^i(\mathbf{r})\}_\ell$ ($\ell = 1, \dots, N_{\text{p}}$), where N_{p} indicates the number of properties of the DM field taken into account. As exposed in Paper I, BAM not only considers the

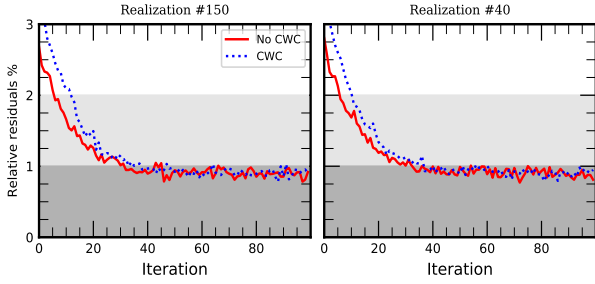


Figure 2. Relative residuals ($\sum_{\kappa} |T_i^{\alpha}(k_{\kappa}) - 1|/N_F$ see § 2.2) for realisations #150 (on the left) and #40 (on the right) demonstrating the fast convergence of BAM after about 30 iterations. Dashed (solid) lines represent calculations with (w/o) cosmic-web classification. Light and dark shadowed areas represent the 2% and 1% deviations, respectively.

local dark matter density as the main halo-bias driver (see e.g. Han et al. 2019, for a recent analysis on the main dependencies of halo-bias), but uses also non-local properties of the A-DMDF by performing, on one side, a cosmic-web classification (e.g. Hahn et al. 2007; Paranjape et al. 2018) and an identification of large-scale collapsing regions (see e.g. Zhao et al. (2015) and Paper I).¹

Explicit third order (or higher) non-local dependencies have not been implemented yet in our method. Although the effects of these elements are absorbed by the kernel, their inclusion could improve the accuracy and precision of the bispectrum, which, given our reference simulation, still displays 5–10% deviations.²

The halo-bias is measured in BAM as

$$\mathcal{B}(N_h | \{\delta_{dm}\}_{\ell}) = \frac{\sum_{i=1}^{N_{\text{cells}}} \mathbf{1}_{N_h}(N_h(\mathbf{r}_i)) \prod_{\kappa=1}^{N_p} \mathbf{1}_{\gamma_{\kappa}}(\{\delta_{dm}(\mathbf{r}_i)\}_{\kappa})}{\sum_{i=1}^{N_{\text{cells}}} \prod_{\kappa=1}^{N_p} \mathbf{1}_{\gamma_{\kappa}}(\{\delta_{dm}(\mathbf{r}_i)\}_{\kappa})}, \quad (1)$$

where $\gamma_{\ell} \equiv [\{\delta_{dm}\}_{\ell} - \Delta_{\ell}/2, \{\delta_{dm}\}_{\ell} + \Delta_{\ell}/2)$ represents the set of bins (of width Δ_{ℓ}) defined for the ℓ -th property of the A-DMDF, with $\mathbf{1}_A(x)$ denoting the *indication function*, $\mathbf{1}_A(x) = 1$ if $x \in A$, 0 otherwise. Note that the conditional probability distribution \mathcal{B} carries no information on the phases of the density fields. Equation (1) is an approximation to the true underlying halo-bias, and ignores key aspects thereof such as the effects of the mass assignment and correlation between pairs in different property-bins, among others. The effects of such missing aspects in the measurement of the bias are nevertheless accounted for within the iterative process, as previously pointed out.

Let us now consider the iterative process in BAM. At the α -th iteration, BAM measures the bias $\mathcal{B}(N_h^{i,\text{ref}} | \{\delta_{adm}^i\}_{\ell})$ using Eq. (1), where $N_h^{i,\text{ref}}$ denotes the halo number counts in cells

¹ The set-up of BAM for this work implements $N_p = 403$ properties spread among the local density (200 bins), 3 cosmic-web types (knots, filaments, sheets+voids) and the mass of collapsing regions M_K (200 bins).

² We note that in Pellejero-Ibañez et. al (in preparation) it is found that choosing a low mass cut of haloes based on high resolution N -body simulations the bispectrum is very well fit, as the galaxy distribution yields a better representation of the dark matter field.

(i.e. using the nearest-grid-point mass assignment scheme) from the high-resolution halo catalogue, and

$$\tilde{\delta}_{adm}^i(\mathbf{r}) \equiv (\mathcal{K}_i^{\alpha-1} \otimes \delta_{dm}^i)(\mathbf{r}) \quad (2)$$

is the convolution of the DMDF with the kernel (in the first iteration, e.g. $\alpha = 1$, the BAM-kernel is simply $\mathcal{K}_i(\mathbf{r}) = \delta_D^3(\mathbf{r})$). With the halo-bias at hand, a HDF (strictly speaking, number counts on a grid) $N_{ah}^i(\mathbf{r})$ is obtained by statistically sampling the density field $\tilde{\delta}_{adm}^i$ as

$$\{N_{ah}^i(\mathbf{r})\} \sim \mathcal{B}(N_h^{i,\text{ref}} | \{\tilde{\delta}_{dm}^i\}_{\ell} = \{\tilde{\delta}_{adm}^i(\mathbf{r})\}_{\ell}), \quad (3)$$

after which its power spectrum $P_{ih}^{\alpha}(k)$, measured in spherical shells characterised by a wave number $k \equiv |\mathbf{k}|$, is used to compute a phase-independent transfer function,

$$\mathcal{T}_i^{\alpha}(k) \equiv \frac{P_h^{i,\text{ref}}(k)}{P_{ih}^{\alpha}(k)}, \quad (4)$$

where $P_h^{i,\text{ref}}(k)$ denotes the power spectrum of the reference halo catalogue. The sampling procedure of Eq. (3) is performed such that the new HDF not only contains the same number of objects as the reference, but also shares its number-count statistics.

For each spherical shell in Fourier space, BAM implements a Metropolis-Hasting (MH) algorithm to accept ($MH = 1$) or reject ($MH = 0$) the corresponding value of the transfer function in Eq. (4) using as metric the quadratic difference of the mock and reference power spectrum in units of the variance thereof, assumed to be a Gaussian (e.g. Feldman et al. 1994). BAM defines a set of weights ω_i^{α} according to the outputs of the MH criteria as:

$$\omega_i^{(\alpha)}(k) \equiv \begin{cases} \mathcal{T}_i^{\alpha}(k) & \text{if } MH = 1 \\ 1 & \text{if } MH = 0, \end{cases} \quad (5)$$

and generates an updated version of the BAM-kernel as a product of the weights at the current step with those from the preceding iterations:

$$\mathcal{K}_i^{(\alpha)}(k) = \prod_{\ell=1}^{\ell=\alpha} \omega_i^{(\ell)}(k) \quad (6)$$

(with $\mathcal{K}_i^{(\alpha=0)}(k) = 1$). This kernel is applied to the A-DMDF, following Eq. (2) to start again with the procedure, as illustrated in Fig. 1.

We characterise the convergence of the iterative procedure by means of the relative residuals $\sum_{\kappa} |T_i^{\alpha}(k_{\kappa}) - 1|/N_F$, where the sum is done over the total number of spherical shells in Fourier space N_F used to measure the different power spectra. Fig. 2 shows the behaviour of these residuals as a function of the number of iterations implemented for calibrations performed using two arbitrarily selected realisations of the Minerva simulations. Ratios below 1% are achieved with approximately ~ 30 iterations, improving to a $< 0.5\%$ for ~ 50 iterations, above which the residuals oscillate around $\leq 1\%$ levels. We have adopted the 1% threshold to stop the iterative process and generate BAM outputs required in the mock-construction.

2.3 Production of mock density fields

The right-hand side panel of Fig. 1 shows the steps followed to generate a mock halo density field based on the outputs

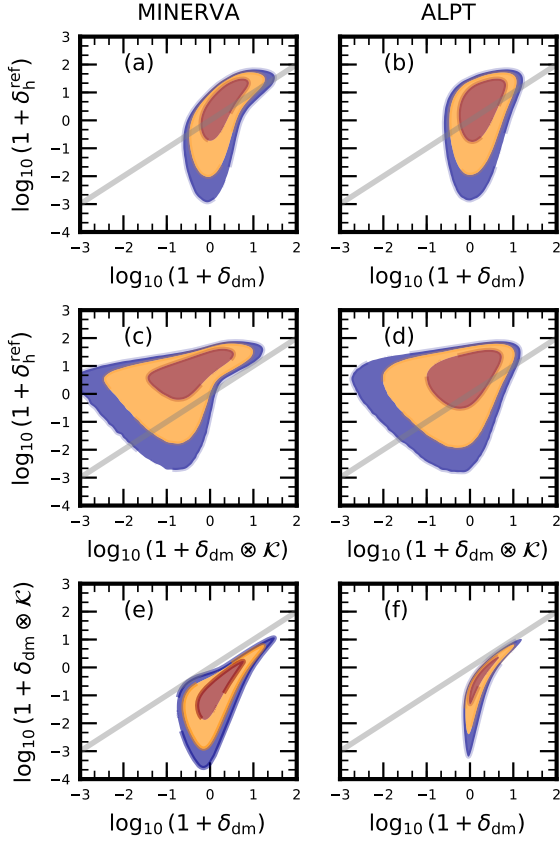


Figure 3. Contours of joint probability distribution in the dark matter - halo plane, from one realisation of the reference simulation, denoting the regions containing the 68% (red), 98% (yellow) and 99% (magenta) of the total number of cells. Panel (a) shows the bias measured from a reference halo catalogue using its corresponding dark matter catalogue. Panel (b) shows the bias obtained from the reference halo catalogue with the approximated dark matter field obtained from ALPT. Panel (c) and (d) show the bias from the reference halo catalogue using the approximated dark matter density field convolved with the BAM kernel using the reference DMDF and the ALPT respectively. Panels (e) and (f) show the relation between the approximated density field and its convolution with the BAM kernel. In all panels the solid line denotes unity bias. Note that the kernels acting in the different columns are different, since these have been calibrated with the different DM fields. For visual purposes, all density fields are obtained using cloud-in-cell interpolation scheme.

from the calibration procedure of BAM, using a new set of realisations of the ICs. We have generated N_{sim} realisations of an A-DMDF δ_{dm}^j ($j = 1, \dots, N_{\text{sim}}$), using the N_{sim} down-sampled versions of the Minerva ICs. These density fields are convolved with the BAM-kernel, $\tilde{\delta}_{\text{dm}}^{j(i\text{ref})}(\mathbf{r}) \equiv (\mathcal{K}_i \otimes \delta_{\text{dm}}^j)(\mathbf{r})$, after which the non-local properties (e.g cosmic-web types) of the resulting field $\tilde{\delta}_{\text{dm}}^{j(i)}$ are determined. According to these properties, BAM statistically populates these fields with a number of haloes as

$$\{N_h^{j(i\text{ref})}(\mathbf{r})\} \sim \mathcal{B}(N_h^{i\text{ref}} | \{\tilde{\delta}_{\text{dm}}^j\}_\ell = \{\tilde{\delta}_{\text{dm}}^{j(i\text{ref})}(\mathbf{r})\}_\ell), \quad (7)$$

where the notation $j(i\text{ref})$ specifies that the j -th halo density field is constructed from the calibration obtained with the

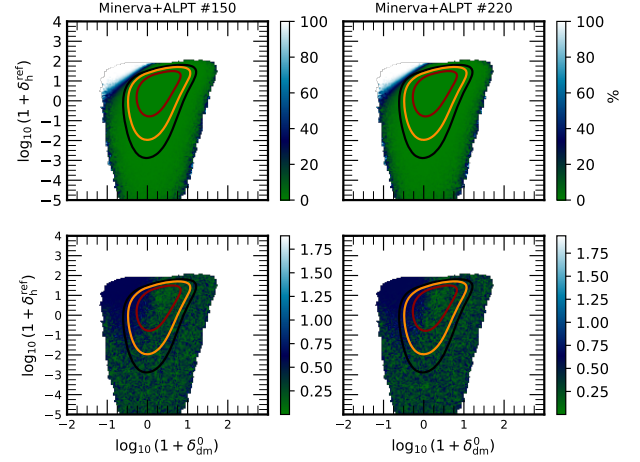


Figure 4. Halo-bias measured from two different realisations of the Minerva simulation and their corresponding white noise evolved using ALPT. The solid lines in all panels denote contours of joint probability distribution (see e.g. Fig. 3). The colour coding in the top-panels indicates the *percent deviation* from the joint distribution $\mathcal{B}(N_h, \delta_{\text{dm}})$ from each particular realisation with respect to the mean obtained from the 300 Minerva+ALPT realisations of halo-bias. The colour coding in the bottom panels represent the deviation from the mean in units of the standard deviation. Differences with respect to the mean are of the order of $\leq 5\%$ in the regions of the $N_h - \delta_{\text{dm}}$ plane containing up top 99.9% of the cells used (black-line contour), and are well below the 1σ level. This indicates that one single simulation contains an accurate bias relation for the considered population of objects.

i -th realisation of the reference simulation. In § 3 we examine the statistical properties of an ensemble of realisations of halo number counts constructed following Eq. (7), assessing their accuracy by comparing them against those of the reference simulation.

Figure 3 displays contours from some of the joint distributions occurring within BAM. Panel (a) shows the halo-bias relation using a high resolution DMDF with its corresponding DMH catalogue. Panel (b) shows the same situation, this time using the A-DMDF generated by ALPT. The stochastic and non-linear behaviour of the halo-bias is evidenced in these two panels, the difference in their shapes being determined by the different DM distributions originated from each gravity solver. In panels (c) and (d) we show how the kernel modifies the 1D-distribution of the DMDF, making it broader towards bins of low DM density, effectively generating a DMDF with a lower clustering amplitude than that from the reference DMDF. Finally, the link between the initial DMDFs and their convolution with BAM kernel is presented in panels (e) and (f) for the reference and the A-DMDF, respectively. Interestingly, the kernel convolution straightens the bias relation, as can be seen comparing the upper panels to the middle ones. Although the scatter in the bias relation is apparently enlarged, we will show below that the covariance matrices are well reproduced. Another key message from Fig. 3 is that the necessity of the iterative process within BAM is not simply due to the approximated nature of the gravity solver used to generate the DMDF to sample from, but also due to the incomplete picture of the halo bias as measured by Eq. (1).

In our approach we need to distinguish among different

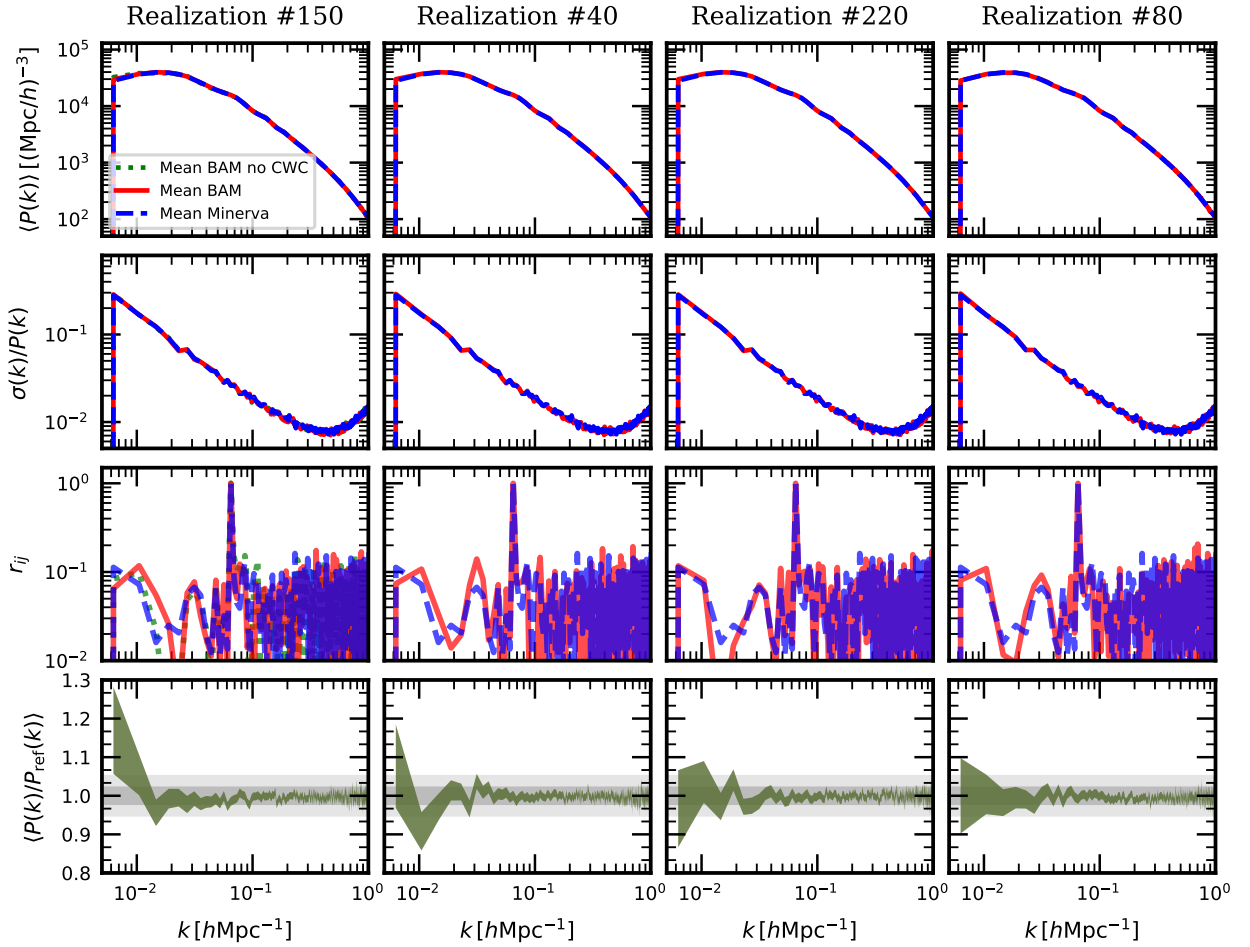


Figure 5. Statistical properties in Fourier space of an ensemble of 300 mock catalogues generated with BAM using *one* reference realisation of the Minerva simulation with their respective DMDF evolved according to the Minerva ICs and ALPT. The different columns show examples of calibrations performed with different references, as highlighted in each plot-title. From top to bottom we present the mean power spectrum, its standard deviation σ in units of the mean power spectrum, one element of the correlation matrix, and the average of the ratio between each realisation to the same realisation in the reference. The solid lines represent the different quantities computed from the BAM mock catalogues. Dotted lines represent the corresponding statistics from the full ensemble of the Minerva simulations. For the calibration performed with the realisation #150 (first column) we show the results of generating mock catalogues without using cosmic-web classification (dotted line). The last row shows the scatter in the ratio between the power spectrum of BAM realisations to the corresponding (according to the IC) power spectrum of the reference ensemble, aimed at assessing the impact of populating different dark matter density fields using the bias and the BAM kernel calibrated from one reference. The shaded areas denote the 2% and 5% differences with respect to unity. This shows that the power spectra are within 2% from $k \sim 0.04 h \text{ Mpc}^{-1}$. However, the impact of cosmic variance can be seen in untreated kernels at lower k .

contributions to the stochasticity in the bias relation. One comes from our effective bias description, relating number counts of objects to the underlying dark matter field on a mesh. This small scale variance can be seen in the scatter of the bias relation in Fig. 3. This contribution is fully accounted for in BAM, as it takes the whole bias relation extracted from reference simulations to assign number counts of objects per cell. Another contribution comes from cosmic variance, as the reference simulation has a limited volume (or equivalently there is a limited number of reference simulations). Due to cosmic variance one has to restrict the study to the halo populations which are well resolved by the reference simulation, as has been done in this study.

We have verified, that the bias relation in the setting of the reference catalogs is well represented by a single simulation (see Fig. 4). Another impact of cosmic variance comes from the spatial distribution of halo number counts, causing noticeable (potentially larger than 10%) deviations from the theoretical mean power spectrum on large scales. This is taken into account within BAM in two steps. The first step, is based on using the same initial conditions (white noise) on large scales, as in the reference simulation. The second step consists on a proper determination of the kernel, as we will study in the next section.

3 BAM AGAINST N-BODY SIMULATIONS

In this section we assess the statistical properties of the ensemble of mocks generated with BAM and compare such properties against those obtained from the reference simulations in Fourier space. In order to demonstrate that BAM is not tailored for any particular realisation of the reference ensemble, we have arbitrarily selected four realisations of ICs and HDFs from the latter, viz, $i = 40, 80, 150$ and $i = 220$. For each one of these, the kernel \mathcal{K} and the bias \mathcal{B} are calibrated as described in § 2.2, and an ensemble of $N_{\text{sim}} = 300$ BAM realisations of HDFs are generated as explained in § 2.3.

3.1 Power spectrum

We first investigate the power spectra from a set of four ensembles of HDF constructed using the calibration performed from the same number of reference simulations, as explained in § 2.3. Figure 5 shows from the first to the third row the ensemble-mean power spectrum, the standard deviation (SD) of the mean and one element of the correlation matrix of the power spectrum, respectively. As can be read from this plot, not only the mean of the BAM ensembles are in excellent agreement with the reference, but also the variance and the correlation matrix are in equally good correspondence. Indeed, the relative residuals (computed as shown in § 2.2) are $\lesssim 1\%$ and $\lesssim 10\%$ for the mean and the standard deviation, respectively. Figure 5 then shows one side that the statistical error budget in the mock power spectra generated with BAM agrees with that of the reference, and that such performance is not due to the implementation of any particular reference simulation.

The bottom panels of Fig. 5 show, with shaded areas, the standard deviation (σ_i) of the ratio between the j -th power spectrum in a BAM set $j(i)$ (i.e. calibrated with the reference i) against the spectrum of the reference associated to the same ICs. This ratio highlights the differences between power spectra of HDFs which, although originated from different gravity solvers (N -body and ALPT) and halo sampling (FoF and BAM), share the same initial conditions. Its standard deviations accounts for the systematic error budget introduced in a set of BAM mocks generated from *one* reference. For the particular set of realisations shown in Fig. 5, this ratio shows values well compatible with unity, except for the largest scales where deviations of $1-2\sigma_i$ are observed, while displaying $\sim 5\%$ random fluctuations on small scales. These deviations are nevertheless below the variance of the ratio of individual realisations to the mean.

3.2 Bispectrum

We now focus on the performance of our set of mocks in terms of the three-point statistics. In Fig. 6 we show the reduced bispectrum $Q(\theta_{12})$ of the BAM mocks, as a function of the angle θ_{12} between the vectors \mathbf{k}_1 and \mathbf{k}_2 with $|\mathbf{k}_2| = 2|\mathbf{k}_1| = 0.2 \text{ Mpc}^{-1}$. The difference between the signal from the BAM ensemble (red shaded region) and that of the reference (blue-shaded regions) is evident, and amounts to ~ 5 times the sample variance. In principle, such discrepancy is likely to be due to unknown dependencies in the halo bias not accounted for in the calibration procedure. This conclusion is motivated by checking the results of running BAM

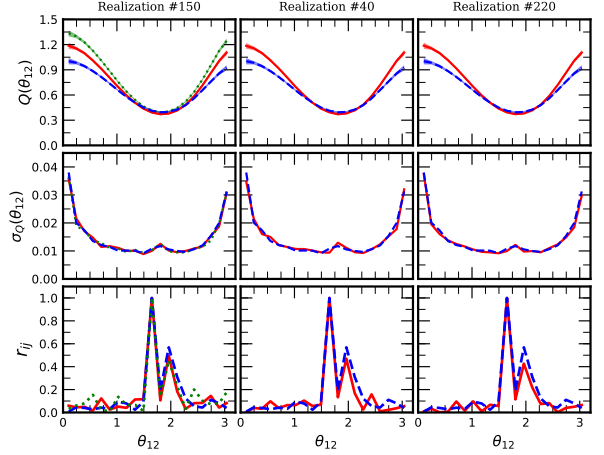


Figure 6. Statistical properties of the BAM mocks in Fourier space in terms of the reduced bispectrum for three different calibrations. In all panels, the blue-dotted (red-solid lines) lines represents the result from the reference (BAM) simulations. The top panels show the mean and sample variance (represented by shaded areas) of the signal for the BAM mocks and the reference. Second and third row show respectively the ensemble standard deviation and one example of the correlation matrix. The first column also shows the results of calibrating the BAM kernel and using a bias which is assumed to be dependent only on the local dark matter density.

assuming a halo-bias to be only a function of the local dark matter density. The first column of Fig. 6 shows the statistics from the set of BAM realisations calibrated without any cosmic-web classification nor environmental dependencies. By construction, the calibration of the power spectrum is not sensitive to the lack of a given set of properties in the characterisation of the halo-bias, since the impact thereof is observed by the kernel. However, the effects of such neglected dependencies in the three-point statistics (which is not calibrated by BAM) are evident, as can be seen in the first column of Fig. 6, where we show the mean bispectra obtained without taking into account any cosmic-web classification (green shaded area). The impact of not considering the cosmic-web information increases the difference with respect to the reference from ~ 4 to ~ 7 times the sample variance. This $\sim 3\sigma$ of difference between the signal with and without cosmic-web information, can be regarded as a signature of non-local bias in the three point statistics, a topic we shall cover in a forthcoming work. It is also interesting that the sample variance in the two cases is in good agreement with that from the reference, as well as the element of the correlation matrix shown. One possible strategy to reproduce the correct three-point signal is to relax the definition of the cosmic-web types by using different values of the threshold (e.g. Forero-Romero et al. 2009), or to increase the dimensionality of our bias measurement in order capture more information of the dark matter density field including e.g. the information of the velocity field. Although no improvement has been reached with the former, we are currently working in including the latter.

In a forthcoming paper (Pellejero-Ibañez et al, in preparation) we show that this discrepancy is also sensitive to the mean number density of the sample (and hence the

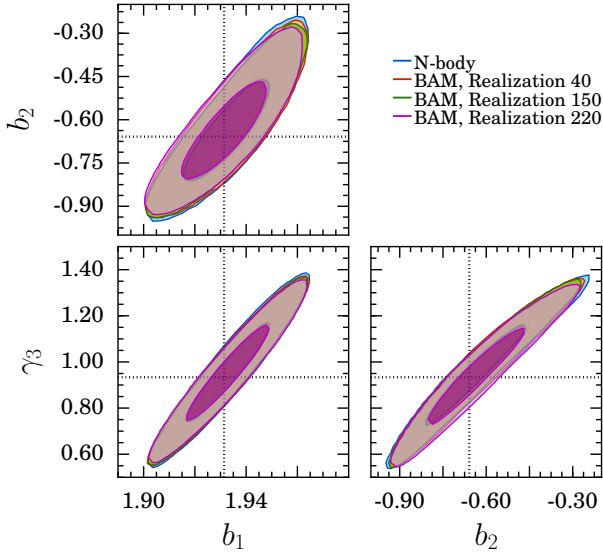


Figure 7. Comparison of the marginalised two-dimensional constraints on the nuisance parameters obtained from the analysis using the covariance matrices from the different BAM catalogues against that from the reference simulations. The contours correspond to the 68% and 95% confidence levels. The dotted lines indicate the expected mean parameter values.

shot-noise level), significantly reducing when applying the method to higher resolution reference simulations. In any case, for the purpose of this work, the discrepancies in the bispectra are small enough to expect accurate covariance matrices of the power spectrum.

3.3 Covariance matrices

In this section we compare the behaviour of the covariance matrix of the power spectrum from the different sets of halo mock catalogues with respect to that from the reference one. We have chosen the BAM sets $j(40)$, $j(150)$ and $j(220)$, and perform fits to the parameters of a given power spectrum model in the likelihood analysis framework. This test goes in the spirit of recent efforts to compare the performance of different approximate methods to generate mock catalogues (Lippich et al. 2019; Blot et al. 2019a; Colavincenzo et al. 2018).

The covariance matrices are computed from the different sets of N_s mock catalogues as $C_{ij} = \langle P_i^k - \langle P_i \rangle_k \rangle \langle P_j^k - \langle P_j \rangle_k \rangle$ where $\langle P_i \rangle_k$ is the mean value of the measurements at the i -th bin and P_i^k is the corresponding measurement from the k -th mock. We take a similar approach to Blot et al. (2019a); Lippich et al. (2019), with the only difference that we focus on the real-space power spectrum covariance, not including redshift-space distortions. We adopt the same model for the real-space power spectrum, which is based on re-normalised perturbation theory (see e.g. Sánchez et al. 2017), containing three free parameters, viz, the linear bias b_1 , the quadratic bias b_2 and the non-local bias parameter γ_3 . All cosmological parameters are kept to their true values, and we use Fourier modes in the range of $0.008 < k/(h\text{Mpc}^{-1}) < 0.25$. We construct synthetic power-spectrum data using the parameters

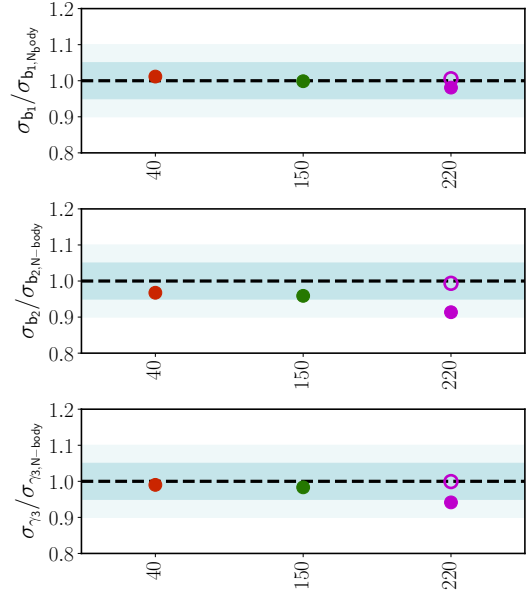


Figure 8. Comparison of the marginalised one-dimensional parameter errors obtained from the analysis using the covariance matrices from the different BAM catalogues against that from the reference simulations. The light grey bands indicate ranges of $\pm 5\%$ and $\pm 10\%$. The empty dot show the errors obtained from the set $j(220)$ constructed with a kernel obtained from the mean of 100 independent calibrations, as discussed in § 3.3.

obtained from the fit of the mean power spectrum measured from the N -body reference halo catalogues with the measured reference covariance matrix and our baseline model. This ensures that our data is perfectly described by our baseline model and differences in the obtained constraints depend only on the covariance matrices. We perform MCMC fits of the theory power spectrum using the four different covariance matrices and assuming a Gaussian likelihood.

Figure 7 shows the two-dimensional marginalised constraints obtained from the analysis with the reference and the three different BAM covariance matrices. We find that the mean parameters resulting from the analysis using the three different BAM covariance matrices are in excellent agreement with the expected parameter values. The resulting 2σ -parameter contours are also well reproduced by the BAM covariance matrices, only for some cases very slightly under- or over-estimating the statistical uncertainties. Therefore, we also consider the one-dimensional marginalised parameter errors drawn from the analysis with the different BAM covariance matrices. Figure 8 shows the ratios of the parameter errors from the results obtained with the BAM mocks with respect to those obtained with the reference. The three BAM covariance matrices reproduce the N -body errors within 10%, in most cases even within 5%, corresponding to the expected statistical limit of our analysis (see Blot et al. 2019a).

We have also constrained the set of parameters for the power spectrum model using the covariance matrix from an ensemble of mock catalogs built with a mean kernel obtained from the calibration of 100 independent kernels. The blank symbols in Fig. 8 show the results obtained from the set built with the halo-bias from reference #220. This approach generates excellent results, with errors which differ $\sim 1\%$ with

those obtained from the reference. We note however that the same procedure is not guaranteed to yield the same results when using the bias calibrated from another realisation. The reason is that any incompatibility between the kernel and the bias is propagated into the error analysis to the off-diagonal elements of the covariance matrix. In other words, the construction of mock catalogs within our method has to be performed with a halo-bias obtained from the same reference used to calibrate the kernel, if precise and accurate covariance matrices are expected to be achieved. The example shown in Fig. 8 for the set $j(220)$ generates good results due to the fortuitous fact that the kernel from the realisation #220 is in good agreement with the mean kernel used to construct that set of mocks.

We have verified that on large scales, the mean kernel is smooth and displays a constant amplitude. While the former property (expected from an average of 100 independent kernels) contributes at reducing the large-scale discrepancies observed in the bottom panels of Fig. 5, the latter opens the possibility to construct mock catalogues with volumes larger than that of the reference simulation, by extrapolating the constant kernel to the desired cosmological volume. Although these conclusions are obtained with 100 independent calibrations, we stress that the same goal can be achieved by mean of the concept of paired-fixed simulations (Angulo & Pontzen 2016; Villaescusa-Navarro et al. 2018; Chuang et al. 2018), consisting in a set of *two* reference simulations generated with the same initial conditions, with fixed amplitude of initial power spectra and inverted phases. As an example, we have verified that using the set described by (Chuang et al. 2018) we obtain a smooth kernel with constant amplitude on large scales. With this approach we also obtain halo-bias corresponding to such kernel, thus providing the perfect scenario for the good performance of the covariance matrices, as we will show in a forthcoming publication.

4 DISCUSSION AND CONCLUSIONS

In this paper we have assessed the accuracy of the recently published Bias Assignment Method (BAM), described in Balaguera-Antolínez et al. (2019) (Paper I). To that aim we have used a reference N -body simulation (the Minerva simulation, Grieb et al. (2016)) and *one* arbitrary member (out of its 300 realisations) in order to calibrate the main outputs of our method. Such outputs (viz, a halo-bias and a kernel) are used to sample 300 dark matter density fields obtained from the evolution of the initial conditions of the reference simulation using Augmented Lagrangian Perturbation Theory (ALPT). This procedure has been repeated using other realisations as references, in order to demonstrate that our method is not tailored for any particular realisation. The halo mock catalogues produced with BAM display power spectra which reproduce the reference ones with 2% precision at $k \sim 0.5h\text{Mpc}^{-1}$ up to 5% precision at the Nyquist frequency $k \sim 1h\text{Mpc}^{-1}$, while the mean of the ensemble agrees to 1% with that from the reference ensemble up to the Nyquist frequency. We have verified that covariance matrices of the two and three point statistics measured from the mock catalogues generated by BAM are in very good agreement with those obtained from the reference N -body simulation. In terms of the power spectrum, such agreement

with the reference is translated into a $\sim 5\%$ difference between the set of uncertainties in parameters of models of power spectrum. Furthermore, we have shown that the implementation of an smooth (on large scales) version of the kernel in conjunction with a compatible bias (i.e, a bias that is calibrated with the kernel from the same reference simulation) can further reduce the differences in the errors to $\sim 1\%$ with respect to those obtained with reference covariance matrix.

The BAM approach is based on the representation of all the non-linear and non-local bias relations in an explicit and parameter free way, extracted from the information of one N -body simulation. In particular, we extract the local and non local properties of the approximated dark matter density field constructed with ALPT. Among such non-local quantities we consider the eigenvalues of the tidal field tensor and the total mass of the collapsed regions (see Paper I). We are fully aware that a series of additional non-local relations are not being accounted for in our description, such as the effective kernel describing a halo finder with respect to our dark matter field representation (in particular the mass assignment kernel of a cloud-in-cell operation) and the missing power of Lagrangian perturbation theory based methods (see e.g. Munari et al. 2017). But even using more accurate gravity solvers, such as FastPm or COLA, as we are using a very low number of particles to describe the dark matter field (for the sake of reducing the computational requirements), we are prone to have some systematic deviations with respect to an accurate representation of the dark matter field, especially towards small scales. Additionally, there are some potential contributions from non-local bias terms which we are not modelling, such as third order contributions (see e.g. McDonald & Roy 2009). Even our second order non-local bias description could still leave some effective aliasing towards small scales, due to, for instance, the particular computation of the eigenvalues (grid resolution, threshold, etc). Since the resulting effective kernel becomes quite complicated, and is unknown in our case, being the sum of all above mentioned effects, we are estimating it iteratively to minimize the deviation from the reference power spectrum. In this way we leave the remainder of the effects we are not explicitly modelling as part of the process involved in the calibration our so-called BAM kernel.

Our method proposes to use *one simulation to have them all*. One such simulation is intended to represent a sufficiently large cosmological volume with dark matter tracers resolved at a high mass resolution, such that the measurements of the halo-bias (e.g. with Eq. (1)) are not dominated by shot-noise. In this framework, large-scale populations of highly biased tracers are to be obtained, not by calibrating the bias and the kernel using low mass resolution (e.g. $\sim 10^{12}M_{\odot}h^{-1}$) simulations, but as sub-samples of BAM mocks constructed from high mass resolution references (see e.g. Zhao et al. 2015). The Minerva simulation offers the scenario in which the (Poisson) signal-to-noise ratio in the halo number counts-per-cells (1 to 3 for a spatial resolution of $3\text{Mpc } h^{-1}$) allows for a significant determination of the halo-bias which in turn permits the convergence of the iterative procedure described in § 2. Nevertheless, the impact of the shot-noise is likely to be propagated into the higher order statistics, partially accounting for the behavior shown in Fig. 6. In Pellejero-Ibañez et al. (in prep) we will show that

higher signal-to-noise ratios in the counts-per-cells lead to much more precise higher order (e.g. three-point) statistics in the **BAM** mocks.

The iterative procedure designed to determine the kernel can be interpreted as a particular case of a machine learning method in which the *cost function* is represented by the power spectrum. Usual deep learning approaches require in general as a training set a large number of catalogues from detailed reference simulations (see e.g. [Mustafa et al. 2017](#); [Mathuriya et al. 2018](#); [He et al. 2018](#)). Such an approach would then capture the nonlinear and non-local effective relation between the halo and the dark matter field. This represents a problem, given that N -body simulations addressing the current galaxy survey requirements are highly demanding (e.g. the Euclid Flagship simulation³). One can certainly go for smaller volumes with techniques such as that suggested by [Angulo & Pontzen \(2016\)](#), but even those are very demanding, and only a few can be done (see e.g. [Chuang et al. 2018](#)). In this work, we use as much information as we have on the physical and statistical relation between the halo and the dark matter distribution to alleviate the need for large training sets.

A second problem of the application of the concepts of machine learning to large scale structure comes from defining the appropriate *cost function*. In this context it is in general dangerous to define as a cost function only the power spectrum, as the bias relation is degenerated at the three-point statistics level (see [Kitaura et al. 2015](#); [Vakili et al. 2017](#)). See, however some interesting recent work using the number counts as the cost function to learn from a single simulation (e.g. [Zhang et al. 2019](#)), as we essentially proposed in Paper I. In **BAM** we can afford restricting our cost function to second order statistics because we do not leave any freedom to the bias relation, which is fully extracted from the reference simulation, as explained above.

Our approach offers the clear advantage of demanding one (at most two) reference simulations as a training set, as well as allowing for the identification of quantities (e.g. the halo-bias and the kernel) encoding physical information (such as assembly bias, e.g. [Zentner \(2007\)](#); [Gao & White \(2007\)](#); [Angulo et al. \(2008\)](#); [Lazeyras et al. \(2017\)](#); [Chue et al. \(2018\)](#); [Contreras et al. \(2019\)](#)) related to the formation and evolution of dark matter tracers. Instead of being competitors, the **BAM** approach and a machine learning technique can be complementary, as an example, at assigning intrinsic properties to the tracers in our mock catalogues, a task we are currently working on.

In summary, our approach extracts the nonlinear and non-local information from a reference simulation, leaving the remaining unknown contributions to a single linear kernel. The method succeeds because a single reference (large enough) simulation encodes a vast information about the bias relation and its dimensionality is effectively given by the number of cells for different density bins, tidal field tensor eigenvalues, and total mass of connected knots. We note, that we can extend our approach to account for third order bias contributions within the same framework, allowing us to improve the precision of the **BAM** mocks in terms of their

three-points statistics. Still a number of issues have to be answered, such as including redshift space distortions, and going to the mass resolution to resolve the haloes hosting emission line galaxies, required for surveys, such as Euclid or DESI. Nevertheless, the present work shows that our method has the potential to generate precise and accurate mock catalogues based on high resolution N -body simulations.

ACKNOWLEDGEMENTS

ABA acknowledges financial support from the Spanish Ministry of Economy and Competitiveness (MINECO) under the Severo Ochoa program SEV-2015-0548. FSK thanks support from grants SEV-2015-0548, RYC2015-18693 and AYA2017-89891-P. MPI acknowledges support from MINECO under the grant AYA2012-39702-C02-01. MPI wishes to acknowledge the contribution of Teide High-Performance Computing facilities for the results of this research. TeideHPC facilities are provided by the Instituto Tecnológico y de Energías Renovables (ITER, SA). REA and MPI acknowledge the Spanish MINECO and the European Research Council through grant numbers *AYA2015-66211-C2-2* and *ERC-StG/716151*, respectively.

REFERENCES

- Abel T., Hahn O., Kaehler R., 2012, *MNRAS*, **427**, 61
 Amendola L., et al., 2016, preprint, ([arXiv:1606.00180](#))
 Angulo R. E., Pontzen A., 2016, *MNRAS*, **462**, L1
 Angulo R. E., Baugh C. M., Lacey C. G., 2008, *MNRAS*, **387**, 921
 Avila S., Murray S. G., Knebe A., Power C., Robotham A. S. G., Garcia-Bellido J., 2015, *MNRAS*, **450**, 1856
 Balaguera-Antolínez A., Kitaura F.-S., Pellejero-Ibáñez M., Zhao C., Abel T., 2019, *MNRAS*, **483**, L58
 Blot L., et al., 2019a, *MNRAS*, p. 500
 Blot L., et al., 2019b, *MNRAS*, **485**, 2806
 Chuang C.-H., Kitaura F.-S., Prada F., Zhao C., Yepes G., 2015, *MNRAS*, **446**, 2621
 Chuang C.-H., et al., 2018, arXiv e-prints, p. [arXiv:1811.02111](#)
 Chue C. Y. R., Dalal N., White M., 2018, *Journal of Cosmology and Astro-Particle Physics*, **2018**, 012
 Colavincenzo M., et al., 2018, *MNRAS*,
 Contreras S., Zehavi I., Padilla N., Baugh C. M., Jiménez E., Lacerna I., 2019, *MNRAS*, **484**, 1133
 Dawson K. S., et al., 2016, *AJ*, **151**, 44
 Dekel A., Lahav O., 1999, *ApJ*, **520**, 24
 Dodelson S., Schneider M. D., 2013, *Phys. Rev. D*, **88**, 063537
 Feldman H. A., Kaiser N., Peacock J. A., 1994, *ApJ*, **426**, 23
 Feng Y., Chu M.-Y., Seljak U., McDonald P., 2016, *MNRAS*, **463**, 2273
 Forero-Romero J. E., Hoffman Y., Gottlöber S., Klypin A., Yepes G., 2009, *MNRAS*, **396**, 1815
 Gao L., White S. D. M., 2007, *MNRAS*, **377**, L5
 Grieb J. N., Sánchez A. G., Salazar-Albornoz S., Dalla Vecchia C., 2016, *MNRAS*, **457**, 1577
 Hahn O., Porciani C., Carollo C. M., Dekel A., 2007, *MNRAS*, **375**, 489
 Hahn O., Abel T., Kaehler R., 2013, *MNRAS*, **434**, 1171
 Han J., Li Y., Jing Y., Nishimichi T., Wang W., Jiang C., 2019, *MNRAS*, **482**, 1900
 He S., Li Y., Feng Y., Ho S., Ravanbakhsh S., Chen W., Póczos B., 2018, arXiv e-prints, p. [arXiv:1811.06533](#)
 Kitaura F.-S., Hess S., 2013, *MNRAS*, **435**, L78

³ <http://sci.esa.int/euclid/59348-euclid-flagship-mock-galaxy-catalogue/>

- Kitaura F.-S., Yepes G., Prada F., 2014, *MNRAS*, **439**, L21
- Kitaura F.-S., Gil-Marín H., Scóccola C. G., Chuang C.-H., Müller V., Yepes G., Prada F., 2015, *MNRAS*, **450**, 1836
- Lazeyras T., Musso M., Schmidt F., 2017, *Journal of Cosmology and Astro-Particle Physics*, 2017, 059
- Leclercq F., Jasche J., Gil-Marín H., Wandelt B., 2013, *J. Cosmology Astropart. Phys.*, **11**, 048
- Levi M., et al., 2013, preprint, ([arXiv:1308.0847](https://arxiv.org/abs/1308.0847))
- Lippich M., et al., 2019, *MNRAS*, **482**, 1786
- Mathuriya A., et al., 2018, arXiv e-prints, p. [arXiv:1808.04728](https://arxiv.org/abs/1808.04728)
- McDonald P., Roy A., 2009, *J. Cosmology Astropart. Phys.*, **8**, 020
- Munari E., Monaco P., Koda J., Kitaura F.-S., Sefusatti E., Borgani S., 2017, *Journal of Cosmology and Astro-Particle Physics*, 2017, 050
- Mustafa M., Bard D., Bhimji W., Lukić Z., Al-Rfou R., Kratochvil J., 2017, arXiv e-prints, p. [arXiv:1706.02390](https://arxiv.org/abs/1706.02390)
- Paranjape A., Hahn O., Sheth R. K., 2018, *MNRAS*, **476**, 3631
- Paz D. J., Sánchez A. G., 2015, *MNRAS*, **454**, 4326
- Percival W. J., et al., 2014, *MNRAS*, **439**, 2531
- Sánchez A. G., et al., 2017, *MNRAS*, **464**, 1640
- Schneider M. D., Ng K. Y., Dawson W. A., Marshall P. J., Meyers J. E., Bard D. J., 2017, *ApJ*, **839**, 25
- Scoccimarro R., Sheth R. K., 2002, *MNRAS*, **329**, 629
- Sigad Y., Branchini E., Dekel A., 2000, *ApJ*, **540**, 62
- Sousbie T., Courtois H., Bryan G., Devriendt J., 2008, *ApJ*, **678**, 569
- Springel V., White S. D. M., Tormen G., Kauffmann G., 2001, *MNRAS*, **328**, 726
- Taylor A., Joachimi B., Kitching T., 2013, *MNRAS*, **432**, 1928
- The Dark Energy Survey Collaboration 2005, ArXiv Astrophysics e-prints,
- Vakili M., Kitaura F.-S., Feng Y., Yepes G., Zhao C., Chuang C.-H., Hahn C., 2017, *MNRAS*, **472**, 4144
- Villaescusa-Navarro F., et al., 2018, *ApJ*, **867**, 137
- Weinberg D. H., 1992, *Monthly Notices of the Royal Astronomical Society*, **254**, 315
- White M., Tinker J. L., McBride C. K., 2014, *MNRAS*, **437**, 2594
- Zentner A. R., 2007, *International Journal of Modern Physics D*, **16**, 763
- Zhang X., Wang Y., Zhang W., Sun Y., He S., Contardo G., Villaescusa-Navarro F., Ho S., 2019, arXiv e-prints, p. [arXiv:1902.05965](https://arxiv.org/abs/1902.05965)
- Zhao C., Kitaura F.-S., Chuang C.-H., Prada F., Yepes G., Tao C., 2015, *MNRAS*, **451**, 4266